IRANIAN JOURNAL OF PHYSICS RESEARCH

Iranian Journal of Physics Research, Vol. 6, No. 3, 2006

# Electron-phonon interaction in high temperature superconductors

**H Khosroabadi, A Tavana, B Mossalla, and M Akhavan***

Magnet Research Laboratory (MRL), Department of Physics, Sharif University of Technology, P.O. Box: 11365-9161, Tehran, Iran
*E-mail: akhavan@sharif.edu

(Received 1 July 2006; in final form 6 November 2006)

**Abstract**
We explore the important role of the strong electron-phonon interaction in high temperature superconductivity through the study of the results of some important experiments, such as inelastic neutron and X-ray scattering, angle resolved photoemission spectroscopy, and isotope effects. We also present our computational results of the eigenvalues and eigenvectors of the $A_g$ Raman modes, and the ionic displacement dependence of the electronic band structure by density functional theory. It is clearly evident that the role of phonons in the mechanism behind the high-temperature superconducting state should be seriously considered.

**Keywords:** HTSC, density functional theory, electronic band structure, $A_g$ Raman modes, electron-phonon interaction

## 1. Introduction

After two decades of enormous research activities since the discovery of high-temperature superconductivity (HTSC) in cuprates [1], although many aspects of the physics and chemistry of the cuprate superconductors are now well understood, the underlying pairing mechanism remains elusive. It is well understood that HTSC is formed by hole or electron doping of the Mott-Hubbard insulating state parent compounds with long-range antiferromagnetic order based on strong Coulomb interaction between electrons [2,3]. It is usually accepted that for HTSCs with the strong electron correlation, the two-dimensional t−J model is a suitable starting point to explain some of the unusual properties both in the normal and superconducting states such as the doping-temperature phase diagram, paring symmetry, pseudogap, etc. [4]. But, these seem not to be sufficient for explaining the mechanism behind the superconducting state in the cuprates.

For a long time, the role of phonons in the pairing mechanism of HTSC has been disregarded. This is despite the existence of many evidences to their relevance, for example the results of isotope experiments. One of the reasons for this was the prevailing belief that phonons simply could not account for such a high transition temperatures ($T_c$). Recent works by inelastic neutron scattering (INS), inelastic X-ray scattering (IXS), angle resolved photoemission spectroscopy (ARPES), and the isotope effects on different properties of these compounds have given clear indications of a strong electron-phonon coupling in various HTSC systems, supporting the debate on the relevance of phonons. These studies indicate that electron-phonon interaction has likely an important role in the properties of HTSCs and maybe in the formation of superconducting state in these compounds. Thus, it seems that the renormalization of strong electron correlation and strong electron-phonon interactions with each other plays a major role in the physics of HTSC cuprates, a new area in condensed matter which has not been studied well. One important question that remaines is how electron-phonon and electron-electron interactions could create the superconducting state in HTSCs.

In this paper, we highlight some experimental and computational results elucidating the importance of the electron-phonon interaction in HTSCs. We begin with some recent experimental studies on the field of electron-phonon interaction like isotope effects, INS, IXS, ARPES, and then, explain our recent computational studies on the phonon spectrum in $GdBa_2Cu_3O_7$ (Gd123), $PrBa_2Cu_3O_7$ (Pr123), $YBa_2Cu_3O_7$ (Y123), and $YBa_2Cu_4O_8$ (Y124), employing the ab-initio density funtional theory (DFT), using the Wien2k and VASP codes.

## 2. Electron-phonon interaction in cuprates

### 2.1 Isotope effect

Although in the early years of the discovery of HTSC the isotope effect was not considered as an important element in the HTSCs, it has now been verified that the unconventional isotope effects observed in the cuprates clearly demonstrate that the electron-phonon interaction plays an important role in the physics of cuprates. Here,

we review briefly some of the important results.

It is now generally accepted that optimally-doped cuprates exhibit a small and positive oxygen-isotope exponent $\alpha_O$ which decreases with increasing $T_c$ [5]. The small oxygen isotope shift observed in the optimally doped cuprates suggests that phonons might not be important in bringing about the high temperature superconductivity, but it increases with decreasing $T_c$ in the underdoped and overdoped systems, and can be even larger than the BCS value in some cases.

By substituting $^{18}O$ for $^{16}O$ in $La_{2-x}Sr_xCuO_4$ (La214), $T_c$ reduces and the isotope exponent $\alpha_O$ increases with a decrease of doping and becomes very large (>0.5) in the deeply underdoped regime [6]. In addition to the large $\alpha_O$ in the underdoped compounds, there are also large $\alpha_{Cu}$ observed in the underdoped La214 [7], oxygen-depleted Y123 [8], Pr-substituted $Y_{1-x}Pr_xBa_2Cu_3O_{7-y}$ and $Y_{1-x}Pr_xBa_2Cu_4O_8$ [9], as well as in Y124 [10]. As $T_c$ or doping decreases, both $\alpha_O$ and $\alpha_{Cu}$ increase monotonously although the $\alpha_{Cu}$ is about 3/4 of $\alpha_O$ in the deeply underdoped region. The large $\alpha_O$ and $\alpha_{Cu}$ suggest that the phonons in the $CuO_2$ planes are more relevant to superconductivity relative to the apical and/or chain oxygen vibrations. To determine the more important oxygen ions in $\alpha_O$, the change of each planar or chain with the isotope can be done and controlled by site-selective oxygen-isotope experiments and confirmed with the Raman data [11-13]. It is also interesting that site-selective oxygen isotope experiments in the underdoped and optimally doped samples of $Y_{1-x}Pr_xBa_2Cu_3O_{7-y}$ remarkably indicate that the planar oxygen ions mainly (>80%) contribute to the total oxygen isotope effect in the optimal and underdoped samples [14,15]. Another important point is that the change of $T_c$ by substituting oxygen is not due to the change of holes, and it is just related to the ionic vibration. There are some experiments which indicate that the change of hole-concentrations after substitution of $^{16}O$ by $^{18}O$ is about 0.0002 per Cu site [16-19]. Also, $T_c$s of the $^{18}O$ samples are always lower than the $^{16}O$ samples by more than 1 K, independent of whether $dT_c/dx$ is positive, negative, or zero.

Susceptibility measurements of the $^{16}O$ and $^{18}O$ samples of undoped La214 and of oxygen doped La214 indicate that the antiferromagnetic (AF) ordering temperature $T_N$ reduces about 1.9 K for substitution of $^{18}O$ for $^{16}O$ in the case of the undoped samples, but the change is negligible in the oxygen doped samples [20]. Temperature dependence of the internal magnetic fields, probed by muon-spin rotation, in $La_{1.97}Sr_{0.03}Cu_{0.98}Mn_{0.02}O_4$ system indicates that the spin-glass freezing temperature $T_g$ almost doubles upon replacing $^{16}O$ by $^{18}O$ [21]. Such a huge isotope effect on $T_N$ and $T_g$, which are neglected in the conventional theories of magnetism in theoretical descriptions of magnetic phenomena, suggests that spin dynamics in cuprates is ultimately correlated with lattice vibrations.

X-ray absorption near edge spectroscopy (XANES) is a powerful technique to probe the local structure conformations for the cuprates, where the charge-stripe formation temperature T* can be determined from the sudden increase of the subtraction of two characteristic XANES peaks. It has been shown that upon replacing $^{16}O$ with $^{18}O$ in $La_{1.94}Sr_{0.06}CuO_4$ system, T* shows a large increase from about 110 K to 180 K [22]. Also, neutron spectroscopic investigation of the $HoBa_2Cu_4O_8$ system [23] indicate that upon replacing $^{16}O$ by $^{18}O$, pseudogap temperature $T_p$ (derived from the deviation of linear temperature dependence of intrinsic linewidth $\Gamma(T)$) changes from 170 K to 220 K. These large dependences of T* and $T_p$ to the isotope effects could also indicate the coupling of charge dynamics and the lattice vibration modes in HTSCs.

The large isotope effect of magnetic penetration depth $\lambda(0)$, derived from diamagnetic Meissner signal in decoupled fine-grained samples, results in a isotope-mass dependence of the average supercarrier mass m* in the $CuO_2$ planes. The Meissner effects for the $^{16}O$ and $^{18}O$ samples of $La_{2-x}Sr_xCuO_4$ with x = 0.06 and 0.105 indicate that there are large oxygen isotope effects on both $T_c$ and the Meissner fraction, i.e. the Meissner fraction of the $^{16}O$ sample reduces about 23% by substitution of $^{18}O$ for x = 0.06 [17,18]. The isotope effects are reversible upon the isotope back-exchange, and reproducible in several sets of samples. Because of a negligible oxygen-isotope effect on the superconducting carrier density $n_s$, a strong isotope dependence of supercarrier mass m* can be concluded from these experiments, since the $\lambda^2(0)$ is proportional to $m^*/n_s$. For x=0.06 sample the value of $\Delta m^*/m^*$ is about 24%, which indicates a large negative oxygen-isotope effect on the effective supercarrier mass in the deeply underdoped cuprates. Highly sensitive torque magnetometer, which is able to detect the small diamagnetic signal for the tiny crystals, confirms these results for single crystal samples [24,25]. The magnetic torque vs. temperature have been measured for $La_{2-x}Sr_xCuO_4$ crystals with x= 0.086 and 0.080 in different $^{16}O$ and $^{18}O$ isotope masses. The relative changes in $T_c$ and $\alpha_O$ are found to be -5.5% and 0.47 for x = 0.080 and -5.1% and 0.40 for x= 0.086, respectively. The relative changes of $\Delta\lambda^2_{ab}(0)/\lambda^2_{ab}(0) \sim \Delta m^*/m^*$ (using $\Delta n_s = 0$) are found to be about 0.9% and 0.7% for x=0.080 and 0.086, respectively [25]. Similar result was also obtained for several optimally doped cuprates $YBa_2Cu_3O_{6.94}$, $La_{1.85}Sr_{0.15}CuO_4$, and $Bi_{1.6}Pb_{0.4}Sr_2Ca_2Cu_3O_{10+y}$ from magnetization measurements [26]. These results are beyond the Migdal theory, where the supercarrier mass is considered as a constant.

The results of different isotope effect experiments indicate that the vibration of oxygen and also Cu ions in the $CuO_2$ plane has an important effect on different electronic, magnetic, and supercounducting properties of HTSC. This indicates that electron-phonon interaction could have an important effect on these properties. Below, we present other evidences to make this more conclusive.

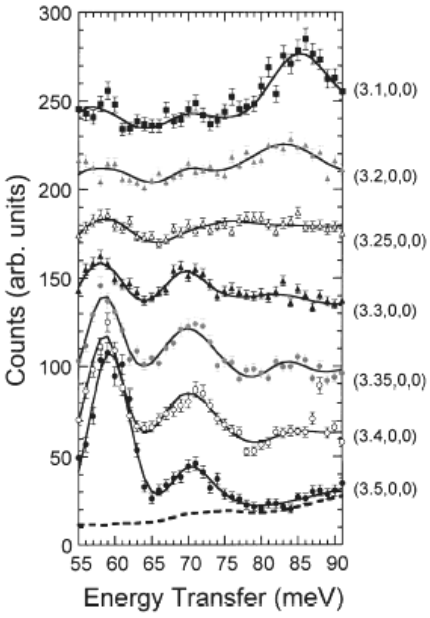


**Figure 1.** Seven energy scans along the (3+$q_x$, 0, 0) direction at 10 K are shown, each successively displaced by 35 counts. Two prominent branches can be tracked from the zone boundary (3.5, 0, 0) point, the in-plane oxygen bond-bending mode at 58 meV and the oxygen bond-stretching mode at 70 meV. The bond-stretching branch experiences a discontinuity at (3.25, 0, 0), jumping to 85 meV as the zone center is approached. Solid lines indicate fits as described in the text. The dashed line for (3.5, 0, 0) is the background obtained from the counting time for each point, assuming a time-independent count rate of 1.4 counts/min (after R.J. McQueeney et al. [35]).

### 2.2. Unusual phonon softening from INS and IXS measurements

Perhaps the most intriguing experimental evidence of a large and anomalous electron-lattice interaction comes from inelastic neutron scattering experiments on various high temperature superconducting materials [27-32]. For example, the strong renormalization (15%–20% softening) of longitudinal high frequency (80 meV) oxygen bond-stretching phonons in the $CuO_2$ plane with hole doping for different HTSC compounds such as $La_{2-x}Sr_xCuO_4$ [27], $La_2CuO_{4+y}$ [29], Y123 [30,31], $Pb_2Sr_2(Ca,Yd)Cu_3O_8$ [33] and $Li_{1+x}Ti_{2-x}O_4$ [34] and even $Ba_{1-x}K_xBiO_3$ [32], indicates that there is a strong coupling of these phonons to the doped holes.

Figure 1 shows an example of these measurements related to a series of longitudinal scans along the (3+$q_x$, 0, 0) direction at T=10 K [35]. Two phonon modes are observed in $q_x$=0.5 at 58 and 70 meV, respectively related to the oxygen in-plane Cu-O bond-bending and the oxygen Cu-O bond-stretching mode in the $CuO_2$ plane. This 70 meV bond-stretching, half-breathing mode is strongly softened as compared to the undoped compound. Inelastic neutron scattering measurements of L214 show that the half-breathing oxygen modes in (ζ, 0, 0) direction soften anomalously from 80 meV (x = 0) to 70 meV (x = 0.15) with doping [27,35]. As can be seen from figure 1, while the frequency of the 58 meV bond-bending branch remains relatively constant through the zone, frequency of the 70 meV branch (remaining constant up until $q_x$=0.25) disappears, and at $q_x$=0.2 a phonon peak reappears at 83 meV, close to the undoped frequency of the phonon branch. So, it can be concluded that, at 10 K, the bond-stretching phonon branch is nearly discontinuous at $q_x$=0.25, with an energy splitting of 13 meV. It has also been found that the dispersion is strongly temperature dependent so that there is a large difference between the values at 10 K and room temperature, not related to the superconducting state [35].

Phonon density of states in $L_{2-x}Sr_xCuO_4$ indicates an abrupt development of new lattice modes near 70 meV with changing of hole concentrations near x = 0.06-0.08, which is related to the doping-induced metal-insulator transition, where trapped holes begin to become mobile. The abrupt change in the DOS is not due to the tetragonal-orthorhombic structural phase transition, and not caused by electrostatic impurity effects from Sr substitution. Thus, the 70 meV band signifies strong and unusual electron-lattice coupling in the metallic state of high temperature superconductors that is not present in the insulating state.

Inelastic X-ray scattering [36] also shows similar anomalous softening along the (ζ, 0, 0) direction for Cu-O bond stretching and out-of-plane oxygen vibration of the electron-doped $Nd_{1.86}Ce_{0.14}CuO_{4+\delta}$ cuprates, such as other hole-doped cuprates [28,29,31,35,37,38], which indicate that this is a generic feature of the high-temperature superconductors. Another IXS also indicate that in nearly optimally doped $HgBa_2CuO_{4+\delta}$ system the Cu-O bond stretching mode at high energy shows strong softening towards the zone boundary, which deviates strongly from the computational model [39].

In summary, as we mentioned in this section, the anomalous softening of the phonon frequencies in HTSCs with doping and wave vector is another evidence for the strong electron-phonon interaction. This is in the direction of isotope effect (see Sec. 2-1) which reveales that electron-phonon interaction could be very important in the electronic properties.

### 2.3. ARPES measurments and phonon collective modes

Recent ARPES measurements have produced a lot of valuable information about the electronic self energy in the both superconducting and normal sates of HTSCs versus the energy and momentum in different temperature and doping regimes [40]. The spectrums have very complex structure, temperature, and doping dependence, and have produced intense discussions about the origin of the superconductivity in HTSCs. These measurements indicate that the kink in the dispersion and the change in the energy dispersive curves width observed along the nodal direction indicate the presence of a well defined energy scale in the electron self energy of HTSCs. This energy scale could be resulted from the coupling between

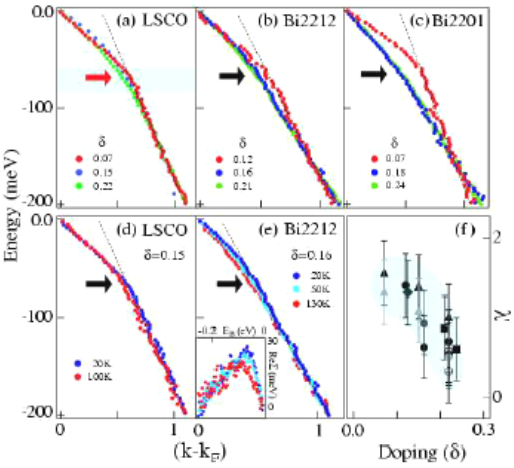


**Figure 2.** (color online) Quasiparticle dispersion of Bi2212, Bi2201 and La214 along the nodal direction, plotted versus the rescaled momentum for different doping (a-c) and temperatures (d,e). The dark arrows in (b-e) indicate the position of the kink, and the light arrow in (a) the energy of the q = (π, 0) oxygen stretching phonon mode. Inset of (e): temperature dependent λ′ for optimally doped Bi2212. (f) Doping dependence of λ′ along (0,0)-(π,π) for all the different cuprates (after A. Lanzara et al. [43]).

the quasiparticles and some collective modes. Due to the large effect of these modes on the electronic dynamics, it can be very important in the electronic physics and also the pairing mechanism of HTSCs. The best two choices for these collective modes are the resonant magnetic-mode [41,42] and the phonon modes [43,44], which have been known as the two important candidates for explanation of the electronic physics of HTSCs.

Figure 2 shows the momentum dependence of quasiparticle dispersion for some HTSCs along the nodal direction and for different values of doping and temperatures [43]. As can be seen from this figure, there is a pronounce energy scale near 70 meV binding energy that changes the behavior of electronic dispersion below and above this energy. Observation of a similar energy scale (50-80meV) in systems with very different gap energies (10-20 meV for La214 and Bi2201, 30-50meV for Bi2212) rules out the superconducting gap as a possible origin. One suitable way is to relate this energy scale to the electron-phonon interactions. This is due to the coupling between quasiparticles and oxygen phonons, which have the same energy for different compounds, and have been obtained from the neutron scattering experiments [35,45]. These lattice vibrational modes are strongly coupled to the charge carriers, and their characteristic frequencies fall in the same energy range of the kink observed in the quasiparticle dispersion.

Furthermore, the similar energy scales in different compounds is a strong evidence against the magnetic-mode interpretation [43], because the magnetic resonant mode behaves very differently: It is not observed in La214, and is expected to have an energy three times lower in Bi2201 as compared to Bi2212 or Y123 due to its scale with $T_c$. Important evidence in favor of the phonon scenario comes from the persistence of the kink in the quasiparticle dispersion well above $T_c$. This is particularly obvious in the 100 K data from La214, for which $T_c$=38 K. The inset in panel (e) presents the real part of the self energy for optimally doped Bi2212 and shows a more continuous evolution, with a persistence of the effect into the normal state. Therefore, the temperature dependence of the ARPES data from Bi2212 and especially La214 [43] is a direct and conclusive evidence against the magnetic-mode interpretation which turns on below $T_c$, as indicated by elastic neutron scattering experiments [46-49].

Figure 2f shows the doping dependence of the electron-phonon coupling parameter λ′. The quantity λ′, which is proportional to the electron-phonon coupling parameter λ (λ′ is already strongly renormalized due to the strong electron-electron correlations over a large energy scale) is estimated from the ratio of the quasiparticle velocities at energies above and below the kink [43]. The doping dependence of λ′ clearly indicates the increase of electron-phonon coupling (as much as 2) in different systems (i.e., La214, Bi2201, and Bi2212) upon reducing the doping level, similar to the isotope effects in HTSCs.

The ARPES results indicate that in addition to the electron self-energy corrections due to electron-electron correlations, which are responsible for the renormalization of the electronic structure of the cuprates over a large energy scale, also the contribution from electron-phonon interaction (which has a direct influence on the quasiparticle dynamics) must be taken into account. In summary, ARPES results indicate a strong electron-phonon interaction in HTSCs which could be very important in the charge dynamics and creation of the superconducting state of these systems.

Secs. 2-1 to 2-3 were devoted to the importance of electron-phonon interaction, even in formation of the superconducting state in HTSCs. So, it seems the electron-phonon interaction cannot be neglected in any real mechanism of superconductivity of HTSCs. So, in the followings, we have carried out some calculations to study the electron-phonon interaction in HTSCs systems.

## 3. Computational studies

In this section we briefly explain the results of our recent calculations on the phonon spectrum, the eigenvalues and eigenvectors of the $A_g$ Raman active modes of some HTSC systems. For our calculations we have used the ab-initio density functional theory (DFT), which is a simple and suitable way to obtain the electronic structure and phonon properties of HTSCs [50]. We also discuss the $A_g$ Raman modes and the ionic displacement dependence of the electronic band structure in Gd123, Pr123, Y123, and Y124 compounds. It should be noted that this is an initial probe to the problem; a more extensive calculation is required for a complete solution.

**Table 1.** Equilibrium lattice parameters, unit cell volume, bulk modulus, and ionic positions for Gd123 and Pr123 in GGA calculation, and for Y123 and Y124 in LDA calculation. The numbers in the second row in each cell indicate the relative percentage difference with the experiment.

| | $a_{eq}$(Å) | $b_{eq}$(Å) | $c_{eq}$(Å) | $V_{eq}$(Å$^3$) | B(GPa) | $Z_{Ba}$ | $Z_{Cu(2)}$ | $Z_{O(2)}$ | $Z_{O(3)}$ | $Z_{O(4)}$ | $Z_{Cu(1)}$ | $Z_{O(1)}$ |
|---|---|---|---|---|---|---|---|---|---|---|---|---|
| Pr123 | 3.881<br>+0.41% | 3.932<br>+0.41 % | 11.735<br>+0.40 % | 179.08<br>+1.22% | 124 | 0.1743 | 0.3523 | 0.3802 | 0.3809 | 0.1635 | --- | --- |
| Gd123 | 3.870<br>+0.42% | 3.919<br>+0.44 % | 11.725<br>+0.42 % | 177.82<br>+1.28 % | 119 | 0.1790 | 0.3558 | 0.3798 | 0.3799 | 0.1618 | --- | --- |
| Y123 | 3.786<br>-1.15 % | 3.836<br>-1.13 % | 11.546<br>-1.15 % | 167.67<br>-3.4 % | 128 | 0.1826 | 0.35365 | 0.3798 | 0.3789 | 0.1597 | --- | --- |
| Y124 | 3.806<br>-1.14 % | 3.826<br>-1.14 % | 26.937<br>-1.15 % | 392.19<br>-3.4 % | 124 | 0.13554 | 0.06125 | 0.0519 | 0.0519 | 0.14565 | 0.2128 | 0.2186 |

### 3.1. Computational details

We have used the Viena Ab-initio Simulation Package (VASP) [51,52] and Wien2k [53,54] computational codes in the local density and generalized gradient approximations (GGA), respectively. The total energy calculations have been performed using ab-initio full potential linear augmented plane wave (in Wien2k) and pseudopotential (in VASP) methods based on DFT. Due to the absence of 4f orbital pseudopotentials of Gd and Pr ions, we have performed the calculations for Gd123 and Pr123 by Wien2k, while for Y123 and Y124 we have used the VASP code. The interaction between ions and electrons is described by ultra-soft Vanderbilt pseudopotentials method in the VASP, and GGA has been used in the Perdew-Burke-Ernzerhof parameterization. The initial lattice parameters and ionic positions for the calculation have been taken from the experimental data [55]. Furthermore, the equilibrium unit cell volume and lattice parameters for the systems have been derived by Murnaghan fitting of the energy-volume data. Then, the ion relaxation has been performed to derive the equilibrium internal positions, by minimizing the ionic forces of the order 0.01 eV/Å, and 0.5 mRy/a.u (~0.01 eV/Å) for VASP and Wien2k, respectively.

The cutoff energy and k-point sampling in the irreducible Brillouin zone are chosen as 400 eV and 50 k for Y123, and 400 eV and 25 k for Y124, respectively. The $R_{MT}\times K_{max}$, $L_{max}$, Broyden factor, and the number of k points in the irreducible wedge of the Brillouin zone have been considered for Wien2k code as 7.0, 10, 0.10 and 72 k, respectively. Performing the calculation for different number of k points, indicates that the number of k points between 100 and 500 sampling in the first Brillouin zone (corresponding to 9 to 72 k points in the irreducible wedge of the Brillouin zone) is sufficient to calculate the total energy of these systems. The total energy has converged in each calculation to better than $10^{-4}$ Ry/(unit cell) for Wien2k and $10^{-4}$ eV/(unit cell) for VASP. The radii of muffin-tin spheres of O, Cu, Ba, Gd, and Pr ions have been considered to be 1.6, 1.8, 2.3, 2.5, and 2.5 a.u., respectively. These values are kept fixed in all of the calculations, and have been chosen such that they remain non-overlapping in the volume optimization and phonon frequency calculation.

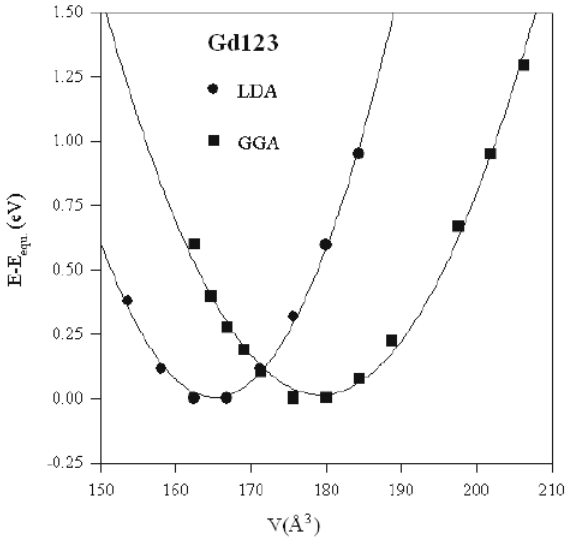


**Figure 3.** The computational data for energy-volume calculation in LDA and GGA for Gd123. The lines show the Murnaghan fitting of the calculated data.

We have calculated the frozen phonon frequencies (at k=0) for the $A_g$ Raman modes of these systems with diagonalization of the dynamical K matrix. Then, the electronic band structure have been calculated for Y123 and Y124 systems in the large symmetric lines of $k_z$=0.0 of the irreducible Brillouin zone for displacement of ionic position in each bare phonon mode. Other computational details can be found in Refs. [56,57].

### 3.2. Results and discussion

The obtained equilibrium lattice parameters (with constant *c*/*a* and *b*/*a* ratio), volume, and ionic positions for Gd123 and Pr123 systems in the GGA, and for Y123 and Y124 in LDA are shown in Table 1. The numbers in parentheses indicate the relative percentage difference with the experiment. The corresponding values in the LDA are *a*=3.770 Å, *b*=3.817 Å, *c*=11.422 Å, and *V*=164.38 Å$^3$ for Gd123, and *a*=3.790 Å, *b*=3.840 Å, *c*=11.460 Å, and *V*=166.79 Å$^3$ for Pr123. The difference between our computational and the experimental data is about 0.41% and 1.25 % for the lattice parameters and the volume, respectively, while the corresponding values are about -2 % and -6 % for the lattice parameters and volume in the

**Table 2.** The eigenvalues and eigenvectors of the $A_g$ Raman active modes of Gd123 system.

| $A_g$ mode | Freq.($cm^{-1}$) | Eigenvectors | | | | |
|---|---|---|---|---|---|---|
| | | Ba | Cu(2) | O(2) | O(3) | O(4) |
| Ba | 102 | 0.58 | 0.78 | 0.17 | 0.16 | -0.01 |
| Cu(2) | 122 | -0.52 | 0.82 | 0.15 | 0.13 | -0.11 |
| O(2)-O(3) | 305 | 0.00 | -0.01 | 0.76 | -0.65 | 0.02 |
| O(2)+O(3) | 358 | -0.01 | -0.05 | 0.59 | 0.70 | 0.41 |
| O(4) | 444 | -0.01 | 0.05 | -0.27 | -0.30 | 0.91 |

**Table 3**. The eigenvalues and eigenvectors of the $A_g$ Raman active modes of Pr123 system.

| $A_g$ mode | Freq.($cm^{-1}$) | Eigenvectors | | | | |
|---|---|---|---|---|---|---|
| | | Ba | Cu(2) | O(2) | O(3) | O(4) |
| Ba | 107 | 0.81 | 0.57 | 0.10 | 0.07 | 0.08 |
| Cu(2) | 125 | -0.31 | 0.94 | 0.11 | 0.07 | -0.06 |
| O(2)-O(3) | 309 | 0.00 | -0.02 | 0.86 | -0.50 | 0.09 |
| O(2)+O(3) | 366 | -0.01 | -0.02 | 0.38 | 0.75 | 0.54 |
| O(4) | 432 | -0.01 | 0.02 | -0.34 | -0.43 | 0.83 |

**Table 4**. The eigenvalues and eigenvectors of the $A_g$ Raman active mode of Y123 system.

| $A_g$ mode | Freq.($cm^{-1}$) | Eigenvectors | | | | |
|---|---|---|---|---|---|---|
| | | Ba | Cu(2) | O(2) | O(3) | O(4) |
| Ba | 103 | 0.55 | 0.81 | 0.13 | 0.12 | -0.08 |
| Cu(2) | 134 | -0.56 | 0.80 | 0.09 | 0.10 | -0.14 |
| O(2)-O(3) | 353 | -0.02 | 0.00 | 0.79 | -0.61 | 0.04 |
| O(2)+O(3) | 394 | -0.01 | -0.03 | 0.52 | 0.70 | 0.49 |
| O(4) | 450 | 0.01 | 0.05 | -0.33 | -0.36 | 0.87 |

**Table 5**. The eigenvalue and eigenvectors of the $A_g$ Raman active mode of Y124 system.

| $A_g$ mode | Freq.($cm^{-1}$) | Eigenvectors | | | | | | |
|---|---|---|---|---|---|---|---|---|
| | | Ba | Cu(1) | Cu(2) | O(1) | O(2) | O(3) | O(4) |
| Ba | 96 | 0.79 | -0.02 | -0.60 | 0.02 | 0.06 | 0.05 | -0.11 |
| Cu(2) | 121 | 0.32 | -0.13 | 0.89 | 0.01 | -0.19 | -0.18 | 0.19 |
| Cu(1) | 250 | 0.05 | 0.96 | 0.12 | 0.13 | 0.10 | 0.04 | -0.19 |
| O(2)-O(3) | 346 | 0.00 | -0.05 | 0.03 | 0.06 | -0.49 | 0.67 | -0.55 |
| O(2)+O(3) | 404 | 0.01 | -0.07 | 0.09 | -0.02 | 0.62 | 0.75 | -0.21 |
| O(4) | 490 | 0.01 | 0.05 | -0.02 | -0.23 | 0.14 | 0.15 | 0.95 |
| O(1) | 585 | 0.00 | -0.02 | -0.01 | 0.97 | 0.04 | 0.05 | 0.23 |

LDA calculation. These results indicate the optimization of calculation under the GGA relative to LDA. The bulk modulus has been derived to be 157 GPa and 119 GPa for Gd123, and 151 GPa and 124 GPa for Pr123 in the LDA and GGA, respectively, and 128.3 and 124 GPa for Y123 and Y124 in LDA, respectively. Figure 3 shows a typical picture for E-V calculations in the LDA and GGA for Gd123, and the Murnaghan fitting of the data. It is evident from the figure that the computational data could be fitted well by the Murnaghan equation of state, which indicates an adequate precision for the calculated data in performing the phonon calculations. This figure also shows that the equilibrium volume in the GGA calculation has been optimized to the experimental value relative to the LDA data. The values obtained for GGA calculation relative to LDA for Wien2k are in good agreement with the reported data for similar systems, and the LDA results of VASP are also in good agreement with the reported data [58,59].

For determining the phonon eigenvalues and eigenvectors of the $A_g$ Raman modes, we have calculated the dynamical K matrix for Ba, Cu(2), O(2), O(3), and O(4) ions which are active in these Raman modes. The diagonal and off diagonal elements have been derived from the total energy and forces versus ionic positions, respectively. For Y123 and Y124, the LDA calculations seems to be adequate for the total energy, phonon frequencies, and band structure calculations, but it is not adequate for systems containing 4f orbital such as Gd or Pr ion. Due to our interest in calculating the phonon frequencies, and not the band structure and the DOS for Gd123 and Pr123, we have not used the LDA+U approach for the 4f states of Gd and Pr ions. Considering constant U for 4f orbitals (independent of the ionic positions which is usually applied for E-V calculation or

**Table 6**. The eigenvalues for the Gd123, Pr123, Y123, and Y124 in comparison with the reported computational and experimental data.

| | This study | | | | Experimental data | | | Computational data | |
|---|---|---|---|---|---|---|---|---|---|
| $A_g$ mode Freq. $cm^{-1}$ | Gd123 | Pr123 | Y123 | Y124 | Y123 [64-67] | Pr123 [68-70] | Y124 [71] | Y123 [60-62] | Y124 [63] |
| Ba | 102 | 107 | 103 | 96 | 110-119 | 115-128 | 103 | 95-123 | 89 |
| Cu(2) | 122 | 125 | 134 | 121 | 145-159 | 149-150 | 150 | 127-147 | 169 |
| Cu(1) | --- | --- | --- | 250 | --- | --- | 247 | --- | 270 |
| O(2)-O(3) | 305 | 309 | 353 | 346 | 330-336 | 298-306 | 340 | 317-338 | 393 |
| O(2)+O(3) | 358 | 366 | 394 | 404 | 435-440 | 430-442 | 439 | 387-422 | 426 |
| O(4) | 444 | 432 | 450 | 490 | 493-500 | 516-529 | 502 | 450-487 | 489 |
| O(1) | --- | --- | --- | 585 | --- | --- | 603 | --- | 576 |

ionic relaxation), could correct the band structure and DOS results for the 4f systems, but in spite of the required large computational time, it makes a marginal contribution to the force and total energy calculations. Therefore, in our phonon calculations we have not considered the U explicitly.

The eigenvalues and eigenvectors of Gd123, Pr123, Y123, and Y124 are shown in Tables 2-5, respectively. From these values we can determine the amplitudes and relative phases of different ions in each mode. For example, for Gd123, Pr123, and Y123 it can be seen that the Ba and Cu(2) ions in the first two modes, known as Ba and Cu(2) modes, are considerably mixed, while there is low mixing of these ions with oxygen ions. Also, the vibrational amplitudes of Ba and Cu(2) ions are small in the three modes of oxygen ions. This indicates that the Ba and Cu(2) ions in the $A_g$ modes of these systems are decoupled from the oxygen ions. The Ba and Cu(2) ions vibrate in the same phase for the Ba mode, while they are in opposite phases in the Cu(2) mode for the two systems. In the O(2)-O(3) mode of these systems O(2) and O(3) ions are in opposite phases, and are decoupled from other ions, while for the O(2)+O(3) mode, O(2) and O(3) ions are in the same phase and couple with the O(4) ion in the same phase.

For Y124, the Cu(1) ion is not mixed with Cu(2), Ba, and other oxygen ions, and thus oscillate alone. In the first mode, the Ba ion is coupled with the Cu(2) ion in opposite phase, while in the second mode they oscillate with each other. In the third mode the Cu(1) ion has the dominant displacement and decouple from the other ions. In the four other modes, the oxygen ions oscillate with each other and are decoupled from the Ba and Cu ions.

Table 6 shows the comparison of our results. It is promising that they are in agreement with other computational studies [60-63] and experimental data [64-71]. Our calculated data are in the range of computational error for these calculations, which is about ten percent. Previous studies in this field indicate that the local density calculated phonon frequencies in the experimental lattice parameters are about ten percent lower than the Raman data. By reducing the experimental lattice parameters to the theoretical equilibrium values, if there is a large difference, all five modes are significantly enhanced and the average discrepancy between the experimental and computational data is reduced [60]. In this study, we have optimized the volume in the GGA, and have found the computational equilibrium volume to be 1.22 % and 1.28 % larger than the experimental value for Pr123 and Gd123 systems, respectively. So, phonon frequency calculations in the optimized volume in GGA of our study increase the difference between the experimental and computational studies by a small amount. This study indicates that the computational phonon frequencies in equilibrium unit cell volume, which is about 6% below the experimental value in LDA, reaches the value of the experimental data. So, if the volume optimization with some correction to the LDA, such as GGA, is obtained near the experimental value, the phonon frequencies have an underestimation of about ten percent. So, maybe doing calculations in the GGA could not refine the ten percent error of the computational data.

This calculation, based on GGA, indicates that $A_g$ eigenvalues do not change considerably after substitution of Gd by Pr ion, and the small differences (highest change is 11 $cm^{-1}$ for the O(4) mode) are within the computational uncertainty (about 2%). It should be noticed that Pr and Gd ions yield different magnetic and electronic properties in the R123 systems. However, the Raman experiments show a marginal difference (less that 5%) in the frequency of $A_g$ phonon modes in these systems. Calculations show that the eigenvalue for the O(4) mode has been decreased by Pr doping, while other frequencies have been increased with Pr doping. Some experimental data, however, show that by Pr substitution, the O(4) mode hardens while the O(2)-O(3) modes softens [68-70].

We have calculated the electronic band structure for Y123 and Y124 systems in the large symmetric lines of the $k_z$=0.0 of the irreducible Brillouin zone for ionic positions of each $A_g$ Raman mode. The details of the results for equilibrium can be found elsewhere in the literature [50,72]. Both of these systems have metallic behaviors such that 4 bands and 8 bands in Y123 and Y124 intersect the Fermi level, respectively. In the following, we analyze the changes of these bands in different $A_g$ Raman modes.

Figures 4-6 show three of these plots for Cu(2), O(3),

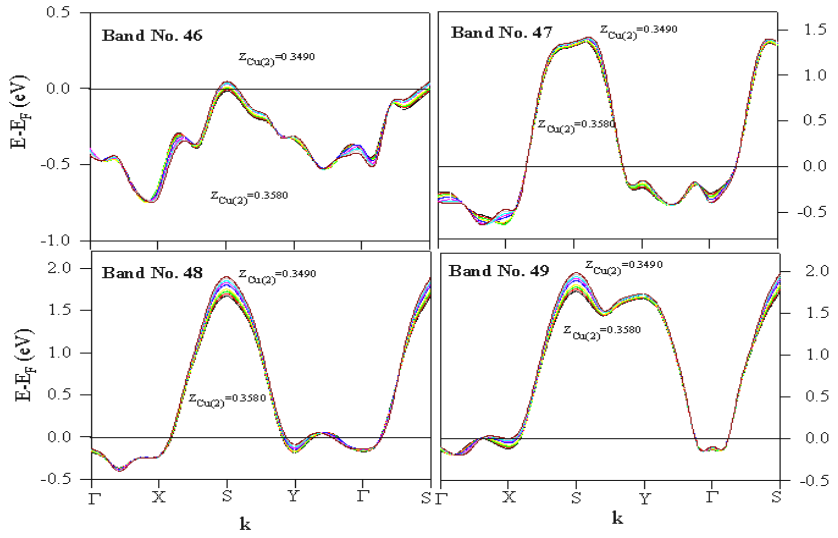


**Figure 4.** (color online) Changes of four bands intersecting the Fermi energy by the change of zCu(2) in Y123.

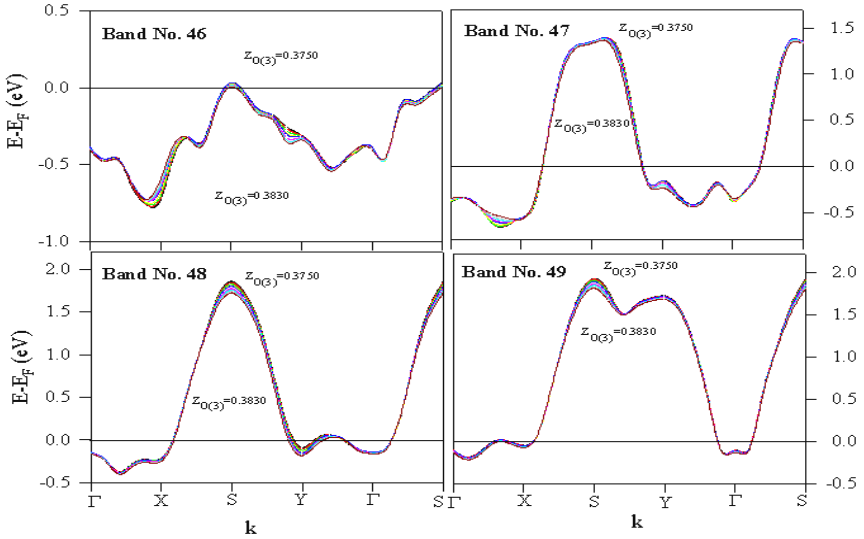


**Figure 5.** (color online) Changes of four bands intersecting the Fermi energy by the change of zO(3) in Y123.

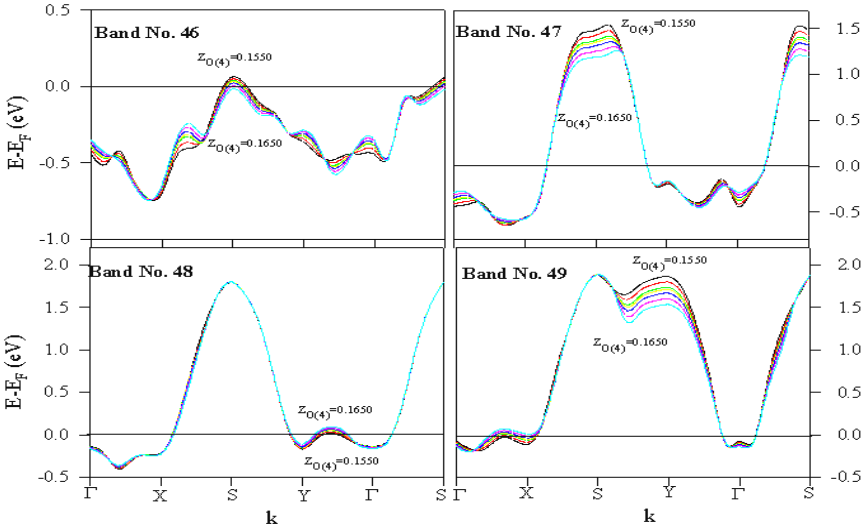


**Figure 6.** (color online) Changes of four bands intersecting the Fermi energy by the change of zO(4) in Y123.

and O(4) displacements, respectively for the four bands intersecting the Fermi level, labeled 46-49 for the Y123 system. The changes of the band structure are gradual with ionic positions, and therefore, the upper and lower limits of each displacement are only shown in the figures. The changes for Ba mode are obtained to be small, and so, it is not shown in the figures. Our results indicate that the coupling of Ba mode with the electronic band structure is small. The changes for the O(2) and O(3) is also near the same, because they have nearly the same position in the compound, and so we have not presented the result for O(2).

One thing apparent in these figures is that some parts of these bands change a lot with displacement of the ionic positions, while other parts change a little or remain the same. For the Cu(2) displacements, the most important changes are near the S point (in the $(\pi,\pi)$ direction of the Fermi surface) in all bands and the X $(\pi,0)$ point for $49^{th}$ band, while the intermediate points change a little. For the S point of the $46^{th}$ band and the X point of the $49^{th}$ band we see the creation of hole carriers with decreasing the zCu(2) which could be very important for the superconducting properties in these systems. This indicates that number of holes could resonate with this phonon mode. The results for O(3) displacements are a little different: The $46^{th}$ and $47^{th}$ bands do not change much, while the most important changes occur in the S point of the $48^{th}$ and $49^{th}$ bands. In this mode, no hole carrier is created or annihilated by the changes of O(3) ionic position. The largest change in these bands is for the O(4) mode. In this mode, the S point of the $46^{th}$ and $47^{th}$ bands, the Y point of the $48^{th}$ and the $49^{th}$ bands, and the X point of the $49^{th}$ band have changed considerably. It can also be seen that the changes near the S point of the $46^{th}$ band annihilate hole carriers by the increase of zO(4), while near the Y point of the $48^{th}$ band and the X point of the $49^{th}$ band hole carriers are created by the increase of zO(4). These changes in the electronic band structure with the ionic position displacement indicate that the hole carriers could couple strongly with the $A_g$ Raman modes.

More than 0.25 eV for the Cu(2) displacement and about 0.4 eV for O(4) displacement indicate large changes of electronic band structure with ionic displacements. Another study has concluded that the hopping parameter *t* is strongly dependent on the ionic positions, in agreement with other studies [73,74]. All of these indications strongly support that hole carriers could couple with the phonon, and that the electron-phonon interaction is strong in these systems. Therefore, it is concluded that the interaction between the ionic positions and the electronic energy in this system is large. This result confirms the experimental and computational studies which believe in the strong electron-phonon interaction in the HTSC compounds.

Our calculations show that the interaction is very anisotropic, and the most interaction occurs in the nodal $(\pi,\pi)$ and antinodal $(0,\pi)$ or $(\pi,0)$ directions of the Fermi surface. This result is in agreement with the ARPES measurements which show anisotropic band renormalization [40]. As can be seen from figures 4-6, the interaction is different for different modes. We find that most changes are for the O(4) and Cu(2) modes, while least changes are for the Ba modes. These calculations are carried out for the bare modes, while for each $A_g$ phonon mode we have a combination of different ionic displacements. The overall results for each mode could be derived from the superposition of these displacements, but this requires an extremely long computational time procedure. So, the changes in the electronic band structure with ionic position are in the bare mode approximation, and to obtain the results for the real phonon modes the contribution of other ions in each mode should be considered.

Similar calculations for Y124 system result again that the band structure is much dependent to the ionic displacement, similar to Y123. Again, like in Y123, the changes for Ba and O(1) are not much and the changes for O(2) and O(3) is nearly the same. Also some special parts of these bands have changed a lot by ionic displacement while the other parts are nearly unchanged. So, we conclude again the strong anisotropic dependence of the electronic band structure to the ionic position in the $A_g$ Raman modes.

## 4. Conclusions

In summary, reviewing different properties of HTSCs indicates that the electron-phonon interaction could be an important interaction in the charge dynamics and also in the mechanism of high temperature superconductivity. Unconventional isotope effects observed in $T_c$, $T_N$, $T_p$, penetration depth, and effective mass of suppercarrier indicate that the electron-phonon interaction in cuprates goes beyond the Midgal theory of strong electron-phonon interaction. The change of $T_c$, $T_N$, $T_p$, and magnetic properties with isotope substitution indicates that phonon is coupled strongly with the charge and spin dynamics. The strong softening of some oxygen modes in the $CuO_2$ plane with hole doping and q for different families of HTSC compounds which have been derived from INS and IXS, are other evidences of the interaction of the phonon modes with electrons. Also, observation of a characteristic energy in ARPES measurements indicates a strong electron-phonon interaction in HTSCs which could be very important in the charge dynamics and creation of the superconducting state of these systems. Our calculations indicate that the density functional theory is a suitable approach to calculate the phonon frequencies, at least in the center of the Brillouin zone, by at most 10 percent difference with the experimental data. The ionic displacement dependence of the electronic band structure also indicates that phonons could be important in the band structure and are strongly coupled with the electrons in these systems.

**Acknowledegement**
This work was supported in part by the Offices of the Vice President for Research and the Dean of Graduate Studies at Sharif University of Technology.

**References**

1. J G Bednorz and K A Mueller, *Z. Phys*. B **64** (1986) 189.
2. P W Anderson, *Science* **235** (1987) 1196.
3. P Monthoux, A V Balatsky and D Pines, *Phys. Rev*. B **46** (1992) 14803.
4. E Dagotto, *Rev. Mod. Phys*. **66** (1994) 763.
5. For example see: G-M Zhao, H Keller and K Conder, *J. Phys. Condens. Matter* (Review article) **13** (2001) R569.
6. G M Zhao, K Conder, H Keller and K A M¨uller, J. *Phys. Condens. Matter*, **10** (1998) 9055.
7. J P Franck, S Harker and J H Brewer, *Phys. Rev. Lett*. **71** (1993) 283.
8. G M Zhao, V Kirtikar, K K Singh, A P B Sinha, D E. Morris and A V Inyushkin, *Phys. Rev*. B **54** (1996) 14956.
9. D E Morris, A P B Sinha, V Kirtikar, K K Singh and A V Inyushkin, *Physica* C **298** (1998) 203.
10. G V M Williams, D J Pringle and J L Tallon, *Phys. Rev*. B **61** (2000) R9257.
11. M Cardona, R Liu, C Thomsen, W Kress, E Sch¨onherr, M Bauer, L Genzel and W Konig, *Solid State Commun*. **67** (1988) 789.
12. W K Ham, S W Keller, J N Michaels, A M Stacey, D Krillov, D T Hodul and R H Fleming, *J. Mater. Res*. **4** (1989) 504.
13. J H Nickel, D E Morris and J W Ager III, *Phys. Rev. Lett*. **70** (1993) 81.
14. D Zech, H Keller, K Conder, E Kaldis, E Liarokapis, N Poulakis and K A Mueller, *Nature* **371** (1994) 681.
15. G M Zhao, J W Ager III and D E Morris, *Phys. Rev*. B **54** (1996) 14982.
16. G M Zhao, K K Singh, A P B Sinha and D E Morris, *Phys. Rev*. B **52** (1995) 6840.
17. G M Zhao, M B Hunt, H Keller and K A Mueller, *Nature* (London) **385** (1997) 236.
18. G M Zhao, K Conder, H Keller and K A Mueller, *J. Phys. Condens. Matter*, **10** (1998) 9055.
19. K Conder, S Rusiecki and E Kaldis, *Mat. Res. Bull*. **24** (1989) 581.
20. G M Zhao, K K Singh and D E Morris, *Phys. Rev*. B **50** (1994) 4112.
21. A Shengelaya, G M Zhao, C M Aegerter, K Conder, I M Savic and H Keller, *Phys. Rev. Lett*. **83** (1999) 5142.
22. A Lanzara, G M Zhao, N L Saini, A Bianconi, K Conder, H Keller and K A Mueller, *J. Phys. Condens. Matter* **11** (1999) L541.
23. D R Temprano, J Mesot, S Janssen, K Conder, A Furrer, H Mutka and K A Mueller, *Phys. Rev. Lett*. **84** (2000) 1990.
24. M Willemin et al., *J. Appl. Phys*. **83** (1998) 1163.
25. J Hofer, K Conder, T Sasagawa, G M Zhao, M Willemin, H Keller and K Kishio, *Phys. Rev. Lett*. **84** (2000) 4192.
26. G M Zhao, V Kirtikar and D E Morris, *Phys. Rev*. B **63** (2001) 220506.
27. L Pintschovius *et al., Physica* (Amsterdam) **185C–189C** (1991) 156.
28. L Pintschovius and W Reichardt, in *Physical Properties of High Temperature Superconductors* Vol. IV, edited by D Ginsberg (World Scientific, Singapore, 1994) 295.
29. L Pintschovius and M Braden, *J. Low Temp. Phys*. **105** (1996) 813.
30. W Reichardt *et al., Physica* (Amsterdam) **162C–164C** (1989) 464.
31. W Reichardt, *J. Low Temp. Phys*. **105** (1996) 807.
32. M Braden *et al., J. Supercond*. **8** (1995) 1.
33. R Currat *et al., Phys. Rev*. B **40** (1989) 11 362.
34. F Gompf, B Renker and H Mutka, *Physica* (Amsterdam) **180B–181B** (1992) 459.
35. R J McQueeney, Y Petrov, T Egami, M Yethiraj, G Shirane and Y Endoh, *Phys. Rev. Lett*. **82** (1999) 628.
36. M d'Astuto, P K. Mang, P Giura, A Shukla, P Ghigna, A Mirone, M Braden, M Greven, M Krisch and F Sette, *Phys. Rev. Lett*. **88** (2002) 167002.
37. L Pintschovius *et al., Physica* (Amsterdam) **174B** (1991) 323.
38. L Pintschovius and M Braden, *Phys. Rev*. B **60** (1999) R15039.
39. H Uchiyama, A Q R Baron, S Tsutsui, Y Tanaka, W-Z Hu, AYamamoto, S Tajima and Y Endoh, *Phys. Rev. Lett*. **92** (2004) 197005.
40. A Damascelli, Z-X Shen and Z Hussain, *Rev. Mod. Phys*. **75** (2003) 473.
41. A Kaminski, M Randeria, J C Campuzano, M R Norman, H Fretwell, J Mesot, T Sato, T Takahashi and K Kadowaki, *Phys. Rev. Lett*. **86** (2001) 1070.
42. P D Johnson, T Valla, A V Fedorov, Z Yusof, B O Wells, Q Li, A R Moodenbaugh, G D Gu, N Koshizuka, C Kendziora, S Jian and D G Hinks, *Phys. Rev. Lett*. **87** (2001) 177007.
43. A Lanzara, P V Bogdanov, X J Zhou, S A Kellar, D L Feng, E D Lu, T Yoshida, H Eisaki, A Fujimori, K Kishio, J-I Shimoyama, T Noda, S Uchida, Z Hussain and Z-X Shen, *Nature* **412** (2001) 510.
44. Z-X Shen, A Lanzara, S Ishihara and N Nagaosa, 2001, *eprint cond-mat*/0108381.
45. Y Petrov, T Egami, R J McQueeney, M Yethiraj, H A Mook and F Do¢gan, 2000, *eprint cond-mat*/0003414.
46. P Dai, H A Mook, S M Hayden, G Aeppli, T G Perring, R D Hunt and F Do¢gan, *Science* **284** (1999) 1344.
47. P Dai, M Yethiraj, F A Mook, T B Lindemer and F Do¢gan, *Phys. Rev. Lett*. **77** (1996) 5425.
48. H F Fong, P Bourges, Y Sidis, L P Regnault, A Ivanov, G D Gul, N Koshizuka and B Keimer, *Nature* **398** (1999) 588.

49. H He, Y Sidis, P Bourges, G D Gu, A Ivanov, N Koshizuka, B Liang, C T Lin, L P Regnault, E Schoenherr and B Keimer, *Phys. Rev. Lett*. **86** (2001) 1610.
50. W E Pickett, *Rev. Mod. Phys*. **61** (1989) 433.
51. G Kresse and J Furthmuller, *Comput. Mater. Sci*. **6** (1996) 15.
52. G Kresse and J Furthmuller, *Phys. Rev*. B **54** (1996) 11169.
53. P Blaha, K Schwarz, G K H Madsen, D Kvasnicka and J Luitz, **Wien2k**, An Augmented Plane Wave + Local Orbitals Program for Calculating Crystal Properties (Karlheniz Schwarz, Techn. Universitat Wien, Austria), 2001. ISBN 3-9501031-1-2.
54. P Blaha, K Schwarz, P Sorantin and B Trickey, *Comput. Phys. Commun*. **59** (1990) 399.
55. R M Hazen in: D M Ginsberg (Ed.), *Physical Properties of High Temperature Superconductors* Vol. II (World Scientific, Singapore, 1990), Chap. 3.
56. A. Tavana, H Khosroabadi and M Akhavan, *Phys. Stat. Sol*. c **3** (2006) 3162.
57. H Khosroabadi, B Mossalla and M Akhavan, *Phys. Stat. Sol*. c **3** (2006) 3140.
58. X J Chen, C D Gong and Y B Yu, *Phys. Rev*. B **61** (2000) 3691.
59. J D Jorgensen, S Pei, P Lightfoot, D G Hinks, B W Veal, B Dabrowski, A P Paulikas and R Kleb, *Physica* C **171** (1990) 93.
60. R Kouba and C Ambrosch-Draxl, B Zangger, *Phys. Rev*. B **60** (1999) 9321.
61. C O Rodriguez, A I Liechtenstein, I I Mazin, O Jepsen, O K Andersen and M Methfessel, *Phys. Rev*. B **42** (1990) R2692.
62. C Ambrosch-Draxl, R Kouba and P Knoll, *Z. Phys*. B **104** (1997) 687.
63. M Cardona, *Physica* C **317-318** (1999) 30.
64. C Thomsen and M Cardona, D M Ginsberg (Ed.), *Physical Properties of High Temperature Superconductors*, Vol. I (World Scientific, Singapore, 1989) 409.
65. T Strach, T Ruf, E Schönherr and M Cardona, *Phys. Rev*. B **51** (1995) 16460.
66. G Burns, F H Dacol, F Holtzberg and D L Kaiser, *Solid State Commun*. **66** (1988) 217.
67. K F McCarty, J Z Liu, R N Shelton and H B *Radousky, Phys. Rev*. B **41** (1990) 8792.
68. A P Litvinchuk, C Thomsen, I E Trofimov, H–U Habermeier and M Cardona, *Phys. Rev*. B **46** (1992) 14017.
69. H B Radousky, K F McCarty, J L Peng and R N Shelton, *Phys. Rev*. B **39** ( 1999) R12383.
70. I-S Yang, G Burns, F H Dacol and C C Tsuei, *Phys. Rev*. B **42** (1990) 4240.
71. E T Heyen, R Liu, C Thomsen, R Kremer and M Cardona, *Phys. Rev*. B **41** (1990) 11058.
72. H Kim and J Ihm, *Phys. Rev*. B **51** (1995) 3886.
73. O Rosch and O Gunnarsson, *Phys. Rev. Lett* **92** (2004) 146403.
74. O Rosch and O Gunnarsson, *Phys. Rev*. B **70** (2004) 224518.